Journal of The Electrochemical Society, **152** (2) A364-A369 (2005)
0013-4651/2005/152(2)/A364/6/$7.00 © The Electrochemical Society, Inc.

Molecular Dynamics Simulations of Li Insertion in a Nanocrystalline V_2O_5 Thin Film Cathode

Weiqun Li and Stephen H. Garofalini[z]

Department of Ceramic and Materials Engineering, Rutgers, The State University, Piscataway, New Jersey 08854, USA

The behavior of lithium ion diffusion from an electrolyte into a polycrystalline layered cathode has been studied using molecular dynamics computer simulations. Lithium silicate glass was the model solid electrolyte while the cathode was a nanocrystalline vanadia with amorphous V_2O_5 intergranular films (IGF) between the crystals. Nanosized V_2O_5 crystals were aligned with their (001) planes parallel to electrolyte/cathode interface, rotated 90° from each other around this interface's normal in order to present two different orientations between the crystal planes for lithium intercalation via the amorphous vanadia IGF. A series of nanocrystalline vanadia cathodes with different IGF thicknesses was simulated to examine the effects of the IGF thickness on lithium transport into the cathodes. Results showed preferential diffusion of Li from the electrolyte into the amorphous vanadia IGF, with some of those Li diffusing into the crystalline V_2O_5 from the IGF. Results also showed easier lithium diffusion from the IGF into the V_2O_5 crystal along the ⟨010⟩ direction than along the ⟨100⟩ direction. Additionally, an optimum IGF thickness of 2.5-3.0 nm is suggested as being neither too thick to decrease the capacity of the cathode nor too thin to impede the transport of lithium from glassy electrolyte into the cathode.
 [DOI: 10.1149/1.1848345]

Manuscript submitted March 24, 2004; revised manuscript received July 5, 2004. Available electronically January 7, 2005.

The transition metal layered oxides have been drawing much attention as a cathode material for advanced rechargeable thin film lithium batteries because of their ability for electrochemical insertion and withdrawal of lithium ions.[1-3] For optimizing the properties of layered oxide cathode materials, such as improving ion conductivity and stabilizing the layered structure, which extends the cyclability and enhances the capacity of lithium batteries, it is important to understand the lithium diffusion process involved in the intercalation reactions. Molecular dynamics (MD) simulations are able to address such questions in detail on the atomistic scale. In this paper, the mechanism of ion transport in one of the prototype layered oxide cathodes, V_2O_5, in a nanocrystalline form is elucidated in the expectation that a better understanding will reveal promising directions for the methods of optimizing the properties of layered oxide cathode materials.

V_2O_5, which has been studied as an optically passive ion storage electrode in electrochromic devices and as a cathode material in thin film batteries, is a good model for understanding lithium ion diffusion in layered oxides.[4-6] The electrochemical performance of crystalline V_2O_5 thin films depends on the nature of its structure and morphology, such as crystal orientation, size of particles, thickness of the intergranular film (IGF), and surface roughness of the substrate.[4] Garcia *et al.* studied the activation energy of the lithium ions diffusing in crystal V_2O_5 as a function of orientation.[7] They found that the activation energy for lithium ion diffusion along the ⟨010⟩ direction of crystal V_2O_5 is low, while there is a much higher activation barrier along the ⟨001⟩ direction. Later, Braithwaite *et al.* got similar results independently using a density functional theory (DFT) derived potential and static lattice simulation techniques.[8] Experimentally deposited vanadia films on solid electrolytes form with the (001) planes parallel to the electrolyte/cathode interface, offering the slow ⟨001⟩ direction to the Li ions from the electrolyte.[9] Thus, nature predisposes the vanadia films on a solid electrolyte glass with the worst possible orientation. However, Garcia *et al.* also observed Li ion transport into amorphous vanadia on par with that for Li transport in the fast ⟨010⟩ direction, implying similar activation barriers.[7] To increase the transport of lithium ions in a V_2O_5 thin film electrode, IGFs of amorphous vanadia between the crystalline vanadia may provide a rapid path for lithium ion diffusion in nanosized polycrystalline V_2O_5.[10]

Nanocrystalline thin film V_2O_5 cathode has two dominant characteristics: small crystallites in which deformation associated with lithium intercalation may be easily relaxed, and high surface area which forms boundaries in the polycrystalline thin film that may be amorphous and may provide high electronic conductivity. The aim of the current work is to study the lithium transport behavior in nanocrystalline V_2O_5 using the molecular dynamics simulation method. The polycrystalline V_2O_5 with different thicknesses of amorphous vanadia IGF formed between two different crystallographic orientations of V_2O_5 nanocrystals are simulated.

Computational Procedure

The development of the interatomic potentials related to the vanadia system and details of the computational procedure have been previously presented.[7,11,12]

A multibody potential containing both pair and three-body terms was used in the simulations

$$V_{\text{total}} = \sum_i \sum_{j>i} V_{ij}^{(2)} + \sum_i \sum_{j\neq i} \sum_{k>j} V_{jik}^{(3)} \quad [1]$$

The two-body term is given as

$$V_{ij}^{(2)} = A_{ij} \exp\left(\frac{-r_{ij}}{\rho_{ij}}\right) + \frac{1}{r_{ij}} q_i q_j \xi\left(\frac{r_{ij}}{\beta_{ij}}\right) + V_{ij}^{\text{CSF}} \quad [2]$$

where r_{ij} is the separation distance between ions i and j, ρ is a softness parameter (in the current work, this is equal to 0.029 nm for all i, j), q is the ion charge, and ξ is the complementary error function erfc. A_{ij} and β_{ij} depend on the ion pairs, i and j. V_{ij}^{CSF} is the additional complementary sigmoidal function (CSF) that takes the form

$$V_{ij}^{\text{CSF}} = \sum_{n=1}^{6} \frac{a_{ij}^n}{1 + \exp[b_{ij}^n (r_{ij} - c_{ij}^n)]} \quad [3]$$

where a_{ij}^n, b_{ij}^n, and c_{ij}^n are empirical parameters which are zero except for those terms given in the tables.

The three-body potential is applied to Si, V, and O central ions, i, and their first-neighbors, j and k, as triplets jik and is defined as

$$V_{jik}^{(3)} = \lambda_{jik} \exp\left(\frac{\gamma_{ij}}{r_{ij} - r_{ij}^0} + \frac{\gamma_{ik}}{r_{ik} - r_{ik}^0}\right) \Omega_{jik} \quad [4]$$

[z] E-mail: shg@glass.rutgers.edu

Table I. Potential parameters of the two-body terms.

Two-body BMH parameters Atom pair		A_{ij} (fJ)	β_{ij} (nm)
Si-O		0.2962	0.234
V-O		0.4450	0.234
Li-O		0.1300	0.240
O-O		0.3200	0.234
Si-Si		0.1877	0.230
V-Si		0.2523	0.230
Li-Si		0.0817	0.230
V-V		0.0500	0.230
Li-V		0.0817	0.230
Li-Li		0.2300	0.230
	$\rho = 0.029$ nm		
Two-body CSF parameters Atom pair		a_{ij}^n (10^{-4} fJ)	b_{ij}^n (nm^{-1})	c_{ij}^n (nm)
V-O	$n = 1$	1.200	1.45	0.324
	2	3.720	1.50	0.260
	3	−1.125	1.00	0.225
	4	1.000	0.240	0.320
	5	−1.650	1.00	0.294
	6	−0.235	1.50	0.346
O-O	$n = 1$	−0.500	1.50	0.280

when $r_{ij} < r_{ij}^0$ and $r_{ik} < r_{ik}^0$. Otherwise $V_{jik}^{(3)} = 0$. λ and γ are fitted parameters. r^0 is the bond length cutoff distance to be considered for a three-body contribution. The angular part, Ω_{jik}, is given by

$$\Omega_{jik} = \left(\cos\theta_{jik} + \frac{1}{3}\right)^2 \quad [5]$$

for Si-O-Si and O-Si-O, and

$$\Omega_{jik} = \left[\left(\cos\theta_{jik} + \frac{1}{3}\right)\sin\theta_{jik}\cos\theta_{jik}\right]^2 \quad [6]$$

for V-O-V and O-V-O, where θ_{jik} is the angle formed by the ions j, i, and k, with the ion i at the vertex.

Table I and II list all the potential parameters used in this paper.

Due to the intercalation of Li ions, the charge of the V ions changed from +5 to ~+4 according to a function that is dependent on V-Li distances and is discussed in detail in conjunction with development of the potential elsewhere.[11] As a Li ion diffused from the electrolyte into the cathode, a new Li ion was introduced into the electrolyte in the volume away from the interface. This kept the charge constant, since the charge on a vanadium ion decreased (implying an imaginary electron entered the cathode) as a Li ion entered the cathode near that vanadium ion. Both constant NVE and NPT simulations were performed.

The processing steps used in the MD simulation for making the V_2O_5 cathode with the amorphous vanadia IGF between ⟨010⟩ and ⟨100⟩ orientated V_2O_5 crystals are outlined in Fig. 1.

The first step involved making two bulk V_2O_5 crystals, each with the ⟨001⟩ parallel to the *Z* direction, but with the crystals oriented

Table II. Three-body parameters.

	r^0 (nm)	λ (10^{-18} J)	γ (nm)
X-O-X[a]	0.26	1.0	0.20
O-Si-O	0.30	24.0	0.28
O-V-O	0.30	20.0	0.28

[a] (X = Si,V)

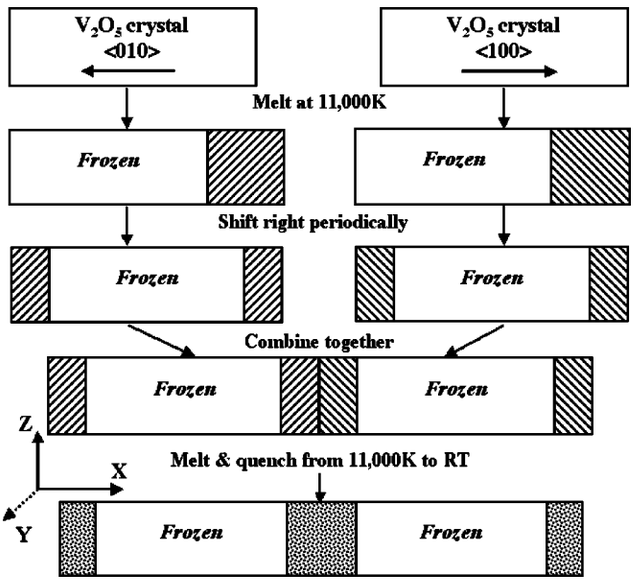

Figure 1. Flow chart of simulation steps for making the amorphous vanadia part of the cathode. Shaded regions are melted and quenched through intermediate temperatures to 300 K to form glassy IGF phase.

such that the ⟨010⟩ and ⟨100⟩ directions of each crystal are given by the arrows in the figure. In order to apply periodic boundary conditions in the combined system later, the number of unit cells along the *Y* axis was carefully selected such that the two differently oriented nanocrystals would each be periodic in the *Y* axis when subsequently combined. The dimensions of the V_2O_5 unit cell are $\vec{a}$ = 11.52 Å, $\vec{b}$ = 3.56 Å and $\vec{c}$ = 4.37 Å.[13] In our simulated V_2O_5 crystals, using a *Y* axis dimension of 46.160 Å enabled both crystals to be periodic in that direction, with four unit cells along $\vec{a}$ in one crystal and 13 unit cells in the other, resulting in these crystals having unit cell dimensions of $\vec{a}$ = 11.5400 Å, $\vec{b}$ = 3.5508 Å, and $\vec{c}$ = 4.3700 Å, which are only slightly different than the ideal values. Periodicity of the crystals in the *X* direction was not in question because of the presence of the amorphous vanadia phases, as discussed below and shown in Fig. 2.

The second step was used to create the amorphous vanadia from the crystal. This was done by keeping the left portion of each crystal frozen and heating the atoms in the right portion to 11,000 K so that they became molten. The frozen parts remained in the crystal structure and were expanded according to the coefficient of thermal expansion of crystal V_2O_5. The nonfrozen part not only expanded according to the coefficient of thermal expansion of amorphous

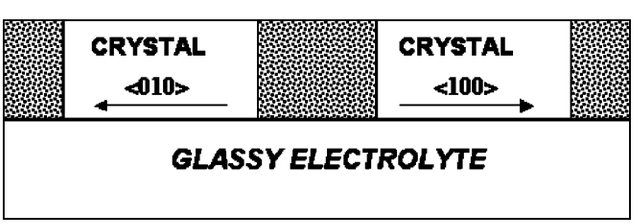

Figure 2. Schematic representation of the structure of the nanocrystalline cathode over the glassy electrolyte. The cathode has two V_2O_5 nanocrystals oriented with their (001) planes parallel to the cathode/electrolyte interface, but rotated 90° from each other along the normal to this interface. This provides two regions for Li intercalation into the crystals through the glassy V_2O_5 IGF, which are shown as the shaded regions. Periodic boundaries exist parallel to the cathode/electrolyte interface.

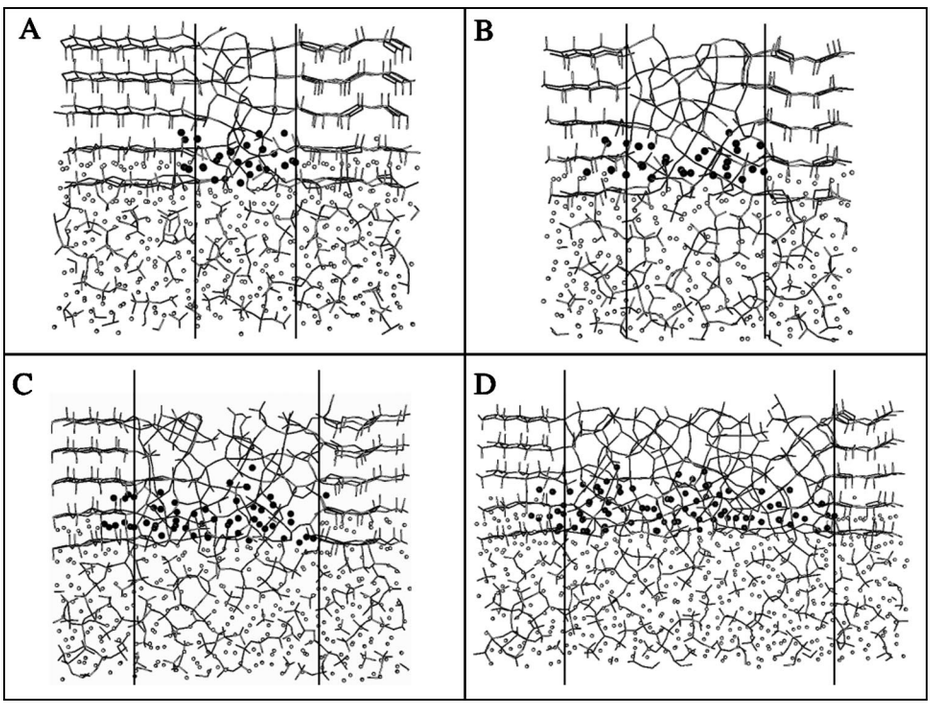

Figure 3. Side views of a thin section (into the page) of cathode/electrolyte interfaces for different thickness IGFs at the end of 7.5×10^5 moves; only Si-O and V-O bonds are drawn. Larger filled circles are Li ions that diffused from the glass electrolyte into the cathode by passing though the IGF(cathode)/electrolyte interface. Smaller, nonfilled circles are Li ions that are still in the glass electrolyte or diffused from the glass electrolyte into the cathode by passing though the crystal(cathode)/electrolyte interface. (A) 1.3, (B) 1.9, (C) 2.9, and (D) 4.4 nm IGF.

V_2O_5, but also expanded according the density change from crystal V_2O_5 to amorphous V_2O_5. This simulation step was performed in constant NPT with periodic boundary conditions applied in three dimensions. The resultant systems were the two crystals, each with an amorphous vanadia connected to it.

The third step involved shifting the two V_2O_5 bulk systems to the right periodically, followed by the fourth step of combining the two bulk systems so that they are continuous along the *X* direction. The dimension of the system in the *X* direction was ~120 Å.

The final step involved remelting and cooling the mobile ions in the IGFs of the combined system from 11,000 K through intermediate temperatures to 300 K, keeping the frozen crystalline parts still frozen. The high temperature allowed the mobile ions in the amorphous vanadia regions to relax in the presence of the now adjacent amorphous vanadia from the other bulk system. The simulation was performed in constant NPT, and periodic boundary conditions were applied in three dimensions. The central amorphous V_2O_5 formed the IGF that was evaluated and discussed in detail in this paper, while the outer sections of amorphous vanadia were used to enable periodic boundary conditions in the *X* direction. While behavior in the central section is discussed in detail, analysis of the other IGF gave results consistent with that shown here. By controlling the frozen atom number and nonfrozen atom number during the initial melt step in the simulation, several IGFs with thicknesses of 1.3, 1.9, 2.9, and 4.4 nm were obtained. (Of course, the frozen atom parts of the crystals were unfrozen in the subsequent simulations.)

The simulated cathode was then interfaced with the Li silicate solid glassy electrolyte, creating the system shown in Fig. 2. The electrolyte/cathode interfaces were formed in the way previously presented.[11]

Density profiles of Li ions that entered the cathode through the IGF as a function of distance perpendicular and parallel to the crystal/IGF interfaces were generated. Density profiles of vanadium ions in different regions of the cathode with the 4.4 nm IGF as a function of distance perpendicular to the crystal/IGF interfaces were also generated. The density profile was taken as the number of ions per unit volume, with the volume given as $y1z1\Delta x$ for the case of distance perpendicular to the crystal/IGF, where $y1$ and $z1$ were the *Y* and *Z* dimensions of the cathode and Δx was the incremental distance perpendicular to the crystal/IGF interface. In the case of the *V* density profiles in the 4.4 nm IGF system, the profiles were taken over specific regions of *x* ($x1$ to $x2$) over all *y* (0 to $y1$) as a function of distance from the cathode/electrolyte interface (Δz), giving a volume element of $y1*(x2\text{-}x1)*\Delta z$.

Results and Discussion

Lithium ion diffusion from the IGF into nanocrystalline V_2O_5.— The Li ions that diffused into the cathode through the IGF/electrolyte interface were given a special pointer to distinguish them from those Li which were still in the glassy electrolyte or that had diffused into the cathode through the crystal V_2O_5/electrolyte interface. Figure 3 presents the side views of the system of small sections of material with four different thicknesses of IGF after 7.5×10^5 moves with the time step of 1.0 fs. The Li ions that passed through the IGF/electrolyte interface are shown as the larger filled circles; the Li ions that were still in the glassy electrolyte or passed through the crystal V_2O_5/electrolyte interface are shown as smaller nonfilled circles.

Even though the images in Fig. 3 are only thin sections of each system, the side views of all four systems revealed that there were Li ions diffusing from the electrolyte into the IGF through the IGF/electrolyte interface and some of these same Li ions diffused from the IGF into the nanocrystal V_2O_5 of the cathode along the ⟨010⟩ direction of the nanocrystal V_2O_5. The potential for Li is deeper (stronger bonding) in the vanadia than the silicate electrolyte glass,[11] acting as the driving force for Li migration into the cathode. Similarly, the potential for Li is slightly deeper in the vanadia crystal than in the amorphous vanadia.[11] Hence, there is still a driving force for Li that have diffused into the amorphous vanadia IGF to further diffuse into the crystalline vanadia.

To better understand the diffusion behavior of Li ions in the whole system, we also studied the density distribution along the *X* axis of Li ions that diffused into the cathode across the IGF/electrolyte interface. Figure 4 shows such density profiles of Li ions in four systems with different thicknesses of IGF after 1.5×10^6 moves. Three interesting features are revealed in this figure: (*i*) Li ion density is higher within the crystal oriented in the ⟨010⟩ direc-

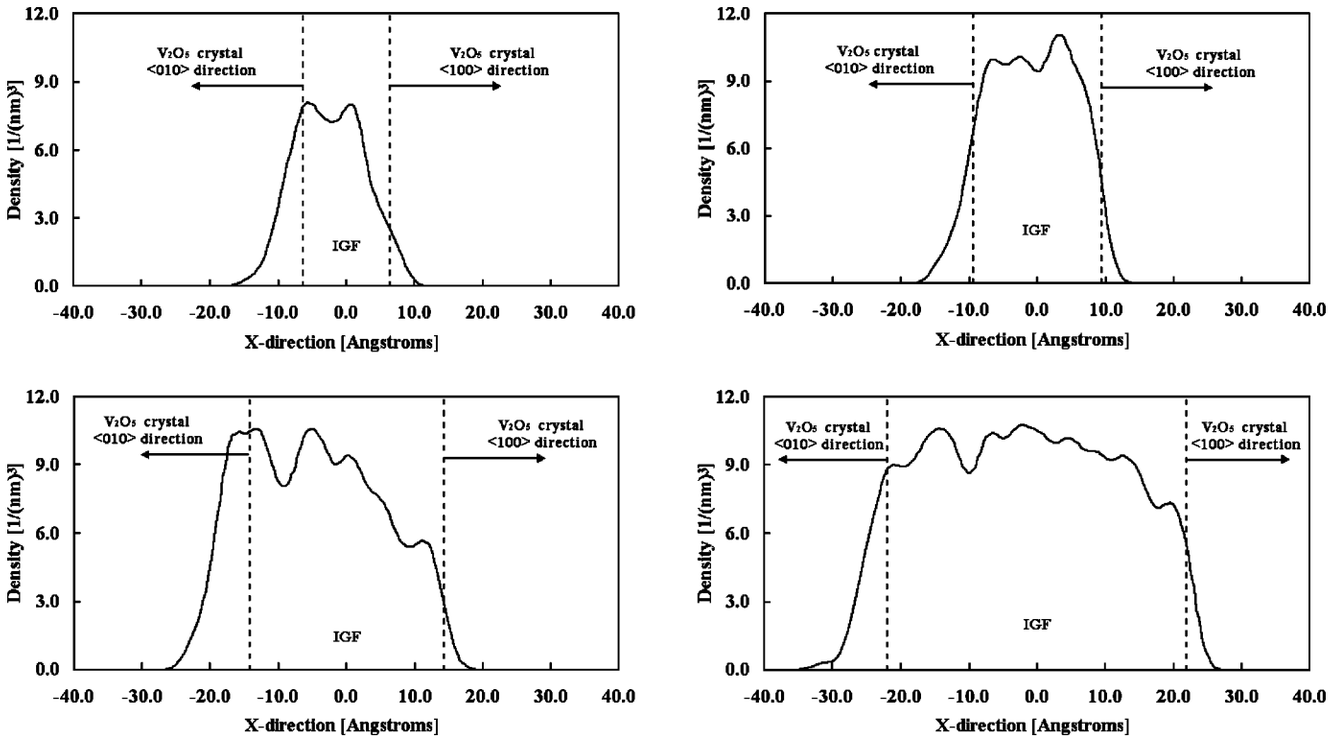

Figure 4. The density profiles of Li ions along the *X* direction in each system. Only Li ions that diffused into the cathode across the IGF/electrolyte interface are shown in order to show the role of the IGF on Li intercalation. A: 1.3, B: 1.9, C: 2.9, and D: 4.4 nm IGF.

tion than the ⟨100⟩ direction, (*ii*) the Li ion density is not symmetrically distributed within the IGF, and (*iii*) the maximum in the Li density increases with the thicker IGFs in comparison to the 1.3 nm IGF.

Considering the first feature, the density distribution of the Li ions along the *X* axis reveals that there are more Li ions diffusing from the IGF into the crystal along the V_2O_5 ⟨010⟩ direction than along V_2O_5 ⟨100⟩ direction. This agrees with the results obtained by Garcia *et al.* that showed lower activation barriers for Li diffusion along the ⟨010⟩ direction than that along the ⟨100⟩ direction.[7,11,12]

In the simulated systems, there were actually two IGFs, the central one at the bottom of Fig. 1 that we are discussing here and the IGF at the ends of the cathode, also in the bottom of Fig. 1, that is not specifically discussed in this paper. The difference of the two IGFs was that they were in a reverse environment, with the ⟨010⟩ direction to the left of one IGF and the $\langle 0\bar{1}0 \rangle$ direction to the right in the other. There should be no difference in the behavior of the two. By checking the Li ion density distribution, the same diffusion behavior was found in the other IGF. So it could be concluded that the faster Li ion diffusing along V_2O_5 ⟨010⟩ (and $\langle 0\bar{1}0 \rangle$) direction than along V_2O_5 ⟨100⟩ (and $\langle \bar{1}00 \rangle$) direction was the result of thermodynamic properties of crystalline V_2O_5.

In Fig. 4, the density distribution of Li ions along *X* axis also revealed that the Li ion density was not symmetrically distributed in the IGF. The density of Li ions in the middle part of the IGF had the highest value, and the density close to ⟨010⟩ oriented V_2O_5 crystal was higher than that close to ⟨100⟩ oriented V_2O_5 crystal. If the structure of the IGF was uniform, Li diffusion into the IGF might be expected to be uniform also. The difference in Li density on the two sides of the IGFs in all cases led to an investigation of the structure of the IGF near the two IGF/crystal interfaces. The structural variation of the IGF was obtained by studying the density profiles of V ions as a function of distance perpendicular to the crystal/IGF interfaces in different regions of the system with the 4.4 nm IGF.

Figure 5 shows the density profiles (a, c) of V as a function of distance perpendicular to the cathode/electrolyte glass interface in different regions of the system with the 4.4 nm IGF system, as well as a snapshot of a thin section of the IGF and the IGF/crystal interfaces (b, d). The snapshot is only for delineating the locations in the *X* dimension over which the V density profiles were taken, as given by the arrows in b and d. Figure 5a shows the density profile of V ions in the crystal (solid line) and in the middle of the IGF (as indicated by the dashed arrow in 5b). The layered structure of the crystal is apparent in the ordered peaks of the V in the crystal. The relatively smooth V profile obtained from V in the middle of the IGF indicates the glassy nature of the amorphous vanadia IGF in this region. Figure 5c shows the density profile of V ions in the 5 Å of the IGF adjacent to the IGF/crystal interface, as indicated in the arrows in 5d. Clearly, the V ions in this region have the peaks more consistent with the crystalline vanadia structure than with the amorphous vanadia structure. This ordering impacts Li diffusion since Li diffusion in the ⟨001⟩ direction has a very high activation barrier, as shown previously.[7] This barrier significantly reduces Li diffusion into the crystal from the electrolyte with the (001) planes parallel to the electrolyte/cathode interface.[12] In addition, the peaks associated with the V ions within 5 Å of the ⟨100⟩ oriented crystal are larger and sharper than those near the ⟨010⟩ oriented crystal. The implication is that the ordering of the V ions in the IGF is greater on the ⟨100⟩ side than the ⟨010⟩ side of the IGF, and this ordering may inhibit Li ion motion into the IGF near the ⟨100⟩ interface more so than near the ⟨010⟩ interface. The effect of this different extent of ordering at the IGF/crystal interfaces is observed in the asymmetry of the Li density profiles given in Fig. 4. The Li concentration in the IGF on the ⟨100⟩ side is lower than that on the ⟨010⟩ side, with the possible cause being the greater crystallinity of the V ions near the ⟨100⟩ side than the ⟨010⟩ side. In addition, there is also the effect of more Li ions diffusing into the ⟨010⟩ oriented crystal from the IGF than into the ⟨100⟩ oriented crystal, because of the lower activation barrier for Li diffusion in the ⟨010⟩ direction. This additional effect

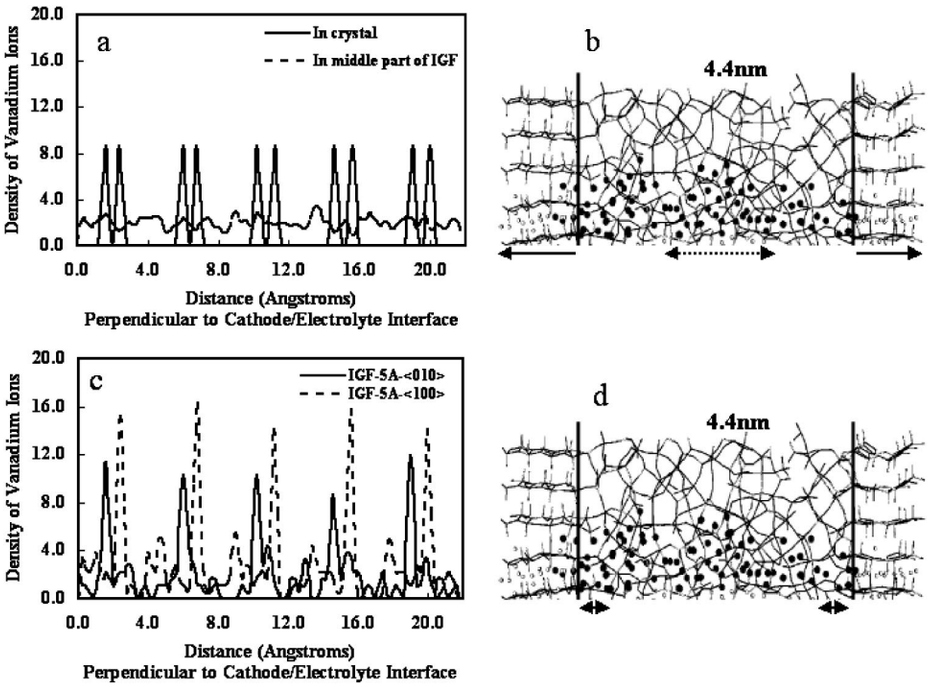

Figure 5. (a,c) Density profiles of V ions as a function of distance perpendicular to the cathode/electrolyte interfaces in different regions of system with the 4.4 nm IGF. (b,d) Snapshots of structure in thin sections to delineate the regions over which the V density profiles were taken. Arrows indicate x dimensions of the sections of IGF and crystal over which the V profiles were collected.

also enhances the concentration of Li ions near the ⟨010⟩ side of the IGF, as some of these diffusing Li are captured in the density profiles. Therefore, the Li concentration on the ⟨010⟩ side of the IGF looks similar to that in the center of the IGF.

The maximum Li concentration is greater in the thicker IGFs than 1.3 nm IGF. This appears to be a consequence of the ordering at the IGF/nanocrystal interfaces, as discussed above, which impedes Li motion within ~0.5 nm of the interface. Of course, the ordering at the IGF/nanocrystal interfaces is not perfect, thus allowing some Li diffusion (otherwise the 1.3 nm IGF would have both ordered sides nearly spanning the full IGF, preventing Li motion similar to the nanocrystals themselves in the ⟨001⟩ direction). This is discussed in more detail below.

The effect of thickness of the IGF on the diffusion of lithium ions.—Figure 6 shows the density profiles of Li ions in the IGF and in the electrolyte directly below the IGF along the Z axis after 1.5×10^6 moves. Li ions show different diffusion behavior with the different IGF thicknesses: in the 1.3 and 1.9 nm IGFs (A and B, respectively), Li ions in the glassy electrolyte directly below the IGF buildup at the IGF/electrolyte interface, as given by the large peak near −2 Å. This Li ion buildup at the IGF/electrolyte interface decreases in the larger IGF systems (C and D). Garcia *et al.* found that there was a buildup of Li ions at the interface between a Li_2SiO_3 glassy electrolyte and the layered V_2O_5 crystal cathode with the (001) planes parallel to the interface; however there was no buildup of Li ions at the interface between a Li_2SiO_3 glassy electrolyte and the amorphous V_2O_5[7] or between the glassy electrolyte and crystalline V_2O_5 oriented with the (001) planes perpendicular to the electrolyte/crystal interface.[7] This buildup of Li at the electrolyte/crystal interface was also discussed with respect to the differently oriented vanadia crystals.[12] The ordering in the IGF induced by the IGF/crystal interfaces makes a fraction of the IGF look more crystalline than otherwise would be expected from a fully amorphous IGF, with the fraction of order being larger for the smaller IGFs. The large peak near +2 Å in the 1.3 nm IGF (curve A in Fig. 6), with a much smaller peak near 6 Å, indicates the extent of ordering in this thin IGF.

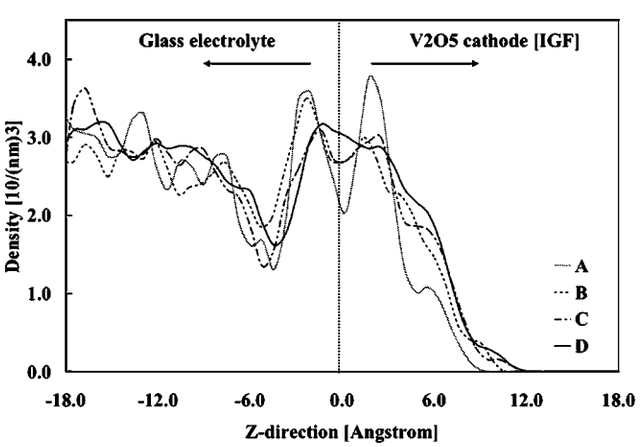

Figure 6. The density profiles of Li ions along the Z direction in the IGF and the glass electrolyte which is just below the IGF after 1.5×10^6 moves. (0.0 marks the normalized location of the lowest V ion.) A: IGF with 1.3 nm thickness; B: IGF with 1.9 nm thickness; C: IGF with 2.9 nm thickness; D: IGF with 4.4 nm thickness.

Another feature seen in Fig. 6 is the limited diffusion of Li in the thinnest IGF, with greater diffusion in the thicker IGFs, although there is not much difference between the two thickest IGFs.

Figure 7 shows the density profiles of Li ions in the crystals, and the 1.3 and 4.4 nm IGFs along the Z axis after 1.5×10^6 moves. From these results, combined with previous data,[7] it appears that in the volume just beneath the IGF, the thinner IGF induces the more crystal-like buildup of Li ions at the IGF/electrolyte interface and crystal-like peaks in the IGF, whereas the thicker IGF induces the amorphous Li-ion behavior at the IGF/electrolyte interface and in the IGF.

Figure 7 shows that the diffusion of Li ions in the IGF was more rapid than that in the nanocrystals from the electrolyte glass. Additionally, the Li ions diffused faster into the 4.4 nm IGF than into the 1.3 nm IGF. However, from Fig. 6, the diffusion of Li ions is about the same in the 2.9 and 4.4 nm IGFs. Thus, 2.9 nm is suggested to be the optimal thickness of the IGF, in that it is neither too thick to

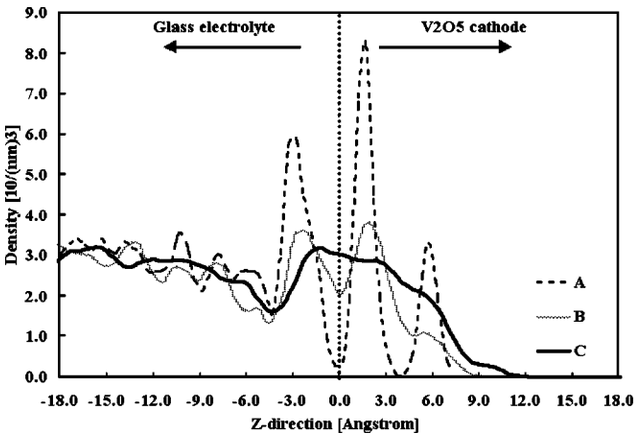

Figure 7. The density profiles of Li ions along *Z* direction after 1.5×10^6 moves. (0.0 marks the normalized location of the lowest V ion.) A: in V_2O_5 crystal and glass electrolyte, which is just under the crystal; B: in IGF with 1.3 nm thickness and glass electrolyte, which is just under the IGF; C: in IGF with 4.4 nm thickness and glass electrolyte, which is just under the IGF.

decrease the capacity of the cathode and nor too thin to inhibit the transport of Li from the glass electrolyte into the nanocrystalline cathode.

Conclusions

Interfacial diffusion of Li ions at the electrolyte/cathode interface and between the amorphous V_2O_5 IGF/nanocrystalline V_2O_5 was studied. Li ions diffuse from the glass electrolyte into the amorphous V_2O_5 IGFs faster than into the ⟨001⟩ orientated V_2O_5 crystal, consistent with expectations from previous work.[7,10] Nonetheless, Li ions can diffuse into the V_2O_5 nanocrystal from the electrolyte via the amorphous V_2O_5 IGF by first diffusing into the IGF, then laterally into the nanocrystals. Also, it is easier for Li ions to diffuse from the IGF into the nanocrystals along the ⟨010⟩ direction at the IGF/nanocrystal interface than along the ⟨100⟩ direction of the V_2O_5 nanocrystals.

An ordered structure of V ions induced by the crystals was found in the IGF near the IGF/nanocrystal V_2O_5 interfaces. This ordering affects Li migration into the otherwise amorphous IGF, having a more significant role in the thinner IGFs than the thicker ones. IGF thickness near 2.9 nm is found to be an optimum thickness for providing rapid transport paths into the nanocrystalline layered vanadia cathode while minimizing the potential loss of capacity that could occur in the amorphous phase.

Acknowledgments

The authors acknowledge support from the U.S. Department of Energy, Office of Science, Basic Energy Sciences, Division of Chemical Sciences, Geosciences, and Biosciences, grant no. DE-FG02-93ER14385.

Rutgers, The State University of New Jersey, assisted in meeting the publication costs of this article.

References

1. G. Prado, L. Fournès, and C. Delmas, *Solid State Ionics*, **138**, 19 (2000).
2. C. Delmas, *Mater. Sci. Eng., B*, **3**, 97 (1989).
3. C. Delmas, C. Fouassier, and P. Hagenmuller, *Physica B & C*, **99**, 81 (1980).
4. A. N. Mansour, P. H. Smith, W. M. Bker, M. Balasubramanian, and J. McBreen, *Electrochim. Acta*, **47**, 3151 (2002).
5. S.-II Pyun, M.-H. Lee, and H.-c. Shin, *J. Power Sources*, **97-98**, 473 (2001).
6. M. D. Levi, Z. Lu, and D. Aurbach, *J. Power Sources*, **97-98**, 482 (2001).
7. M. Garcia and S. H. Garofalini, *J. Electrochem. Soc.*, **146**, 840 (1999).
8. J. S. Braithwaite, C. R. A. Catlow, and J. H. Harding, *Chem. Mater.*, **11**, 1990 (1999).
9. A. E. Semenov, I. N. Borodina, and S. H. Garofalini, *J. Electrochem. Soc.*, **148**, A1239 (2001).
10. S. H. Garofalini, *J. Power Sources*, **110**, 412 (2002).
11. M. Garcia, E. Webb, and S. H. Garofalini, *J. Electrochem. Soc.*, **145**, 2155 (1998).
12. S. H. Garofalini and P. Shadwell, *J. Electrochem. Soc.*, **83**, 2273 (2000).
13. R. W. G. Wyckoff, *Crystal Structures*, 2d ed., New York: Interscience Publishers, New York (1963).